



Year: 2019

18F-AzaFol for Detection of Folate Receptor- Positive Macrophages in Experimental Interstitial Lung Disease-A Proof-of-Concept Study

Schniering, Janine ; Benešová, Martina ; Brunner, Matthias ; Haller, Stephanie ; Cohrs, Susan ; Frauenfelder, Thomas ; Vrugt, Bart ; Feghali-Bostwick, Carol ; Schibli, Roger ; Distler, Oliver ; Müller, Cristina ; Maurer, Britta

Abstract: Background: Interstitial lung disease (ILD) is a common and severe complication in rheumatic diseases. Folate receptor- is expressed on activated, but not resting macrophages which play a key role in dysregulated tissue repair including ILD. We therefore aimed to pre-clinically evaluate the potential of ¹⁸F-AzaFol-based PET/CT (positron emission computed tomography/computed tomography) for the specific detection of macrophage-driven pathophysiologic processes in experimental ILD. Methods: The pulmonary expression of folate receptor- was analyzed in patients with different subtypes of ILD as well as in bleomycin (BLM)-treated mice and respective controls using immunohistochemistry. PET/CT was performed at days 3, 7, and 14 after BLM instillation using the ¹⁸F-based folate radiotracer ¹⁸F-AzaFol. The specific pulmonary accumulation of the radiotracer was assessed by ex vivo PET/CT scans and quantified by ex vivo biodistribution studies. Results: Folate receptor- expression was 3- to 4-fold increased in patients with fibrotic ILD, including idiopathic pulmonary fibrosis and connective tissue disease-related ILD, and significantly correlated with the degree of lung remodeling. A similar increase in the expression of folate receptor- was observed in experimental lung fibrosis, where it also correlated with disease extent. In the mouse model of BLM-induced ILD, pulmonary accumulation of ¹⁸F-AzaFol reflected macrophage-related disease development with good correlation of folate receptor- positivity with radiotracer uptake. In the ex vivo imaging and biodistribution studies, the maximum lung accumulation was observed at day 7 with a mean accumulation of $1.01 \pm 0.30\%$ injected activity/lung in BLM-treated vs. control animals ($0.31 \pm 0.06\%$ injected activity/lung; $p < 0.01$). Conclusion: Our preclinical proof-of-concept study demonstrated the potential of ¹⁸F-AzaFol as a novel imaging tool for the visualization of macrophage-driven fibrotic lung diseases.

DOI: <https://doi.org/10.3389/fimmu.2019.02724>

Posted at the Zurich Open Repository and Archive, University of Zurich

ZORA URL: <https://doi.org/10.5167/uzh-178860>

Journal Article

Published Version



The following work is licensed under a Creative Commons: Attribution 4.0 International (CC BY 4.0) License.

Originally published at:

Schniering, Janine; Benešová, Martina; Brunner, Matthias; Haller, Stephanie; Cohrs, Susan; Frauenfelder, Thomas; Vrugt, Bart; Feghali-Bostwick, Carol; Schibli, Roger; Distler, Oliver; Müller, Cristina; Maurer, Britta (2019). ¹⁸F-AzaFol for Detection of Folate Receptor- Positive Macrophages in Experimental Interstitial Lung Disease-A Proof-of-Concept Study. *Frontiers in Immunology*, 10:2724.
DOI: <https://doi.org/10.3389/fimmu.2019.02724>



¹⁸F-AzaFol for Detection of Folate Receptor-β Positive Macrophages in Experimental Interstitial Lung Disease—A Proof-of-Concept Study

OPEN ACCESS

Edited by:

Kutty Selva Nandakumar,
Southern Medical University, China

Reviewed by:

Philip S. Low,
Purdue University, United States
Adriaan Anthonius Lammertsma,
VU University Medical
Center, Netherlands

*Correspondence:

Cristina Müller
cristina.mueller@psi.ch
Britta Maurer
britta.maurer@usz.ch

†These authors have contributed
equally to this work

Specialty section:

This article was submitted to
Autoimmune and Autoinflammatory
Disorders,
a section of the journal
Frontiers in Immunology

Received: 14 August 2019

Accepted: 06 November 2019

Published: 22 November 2019

Citation:

Schniering J, Benešová M, Brunner M,
Haller S, Cohrs S, Frauenfelder T,
Vrugt B, Feghali-Bostwick C,
Schibli R, Distler O, Müller C and
Maurer B (2019) ¹⁸F-AzaFol for
Detection of Folate Receptor-β
Positive Macrophages in Experimental
Interstitial Lung Disease—A
Proof-of-Concept Study.
Front. Immunol. 10:2724.
doi: 10.3389/fimmu.2019.02724

Janine Schniering¹, Martina Benešová^{2,3}, Matthias Brunner¹, Stephanie Haller²,
Susan Cohrs², Thomas Frauenfelder⁴, Bart Vrugt⁵, Carol Feghali-Bostwick⁶,
Roger Schibli^{2,3}, Oliver Distler¹, Cristina Müller^{2,3*†} and Britta Maurer^{1*†}

¹ Department of Rheumatology, Center of Experimental Rheumatology, University Hospital Zurich, Zurich, Switzerland, ² Center for Radiopharmaceutical Sciences, Paul Scherrer Institute, Villigen, Switzerland, ³ Department of Chemistry and Applied Biosciences, ETH Zurich, Zurich, Switzerland, ⁴ Institute of Diagnostic and Interventional Radiology, University Hospital Zurich, Zurich, Switzerland, ⁵ Institute of Pathology and Molecular Pathology, University Hospital Zurich, Zurich, Switzerland, ⁶ Division of Rheumatology & Immunology, Medical University of South Carolina, Charleston, SC, United States

Background: Interstitial lung disease (ILD) is a common and severe complication in rheumatic diseases. Folate receptor-β is expressed on activated, but not resting macrophages which play a key role in dysregulated tissue repair including ILD. We therefore aimed to pre-clinically evaluate the potential of ¹⁸F-AzaFol-based PET/CT (positron emission computed tomography/computed tomography) for the specific detection of macrophage-driven pathophysiologic processes in experimental ILD.

Methods: The pulmonary expression of folate receptor-β was analyzed in patients with different subtypes of ILD as well as in bleomycin (BLM)-treated mice and respective controls using immunohistochemistry. PET/CT was performed at days 3, 7, and 14 after BLM instillation using the ¹⁸F-based folate radiotracer ¹⁸F-AzaFol. The specific pulmonary accumulation of the radiotracer was assessed by *ex vivo* PET/CT scans and quantified by *ex vivo* biodistribution studies.

Results: Folate receptor-β expression was 3- to 4-fold increased in patients with fibrotic ILD, including idiopathic pulmonary fibrosis and connective tissue disease-related ILD, and significantly correlated with the degree of lung remodeling. A similar increase in the expression of folate receptor-β was observed in experimental lung fibrosis, where it also correlated with disease extent. In the mouse model of BLM-induced ILD, pulmonary accumulation of ¹⁸F-AzaFol reflected macrophage-related disease development with good correlation of folate receptor-β positivity with radiotracer uptake. In the *ex vivo* imaging and biodistribution studies, the maximum lung accumulation was observed at day 7 with a mean accumulation of 1.01 ± 0.30% injected activity/lung in BLM-treated vs. control animals (0.31 ± 0.06% % injected activity/lung; *p* < 0.01).

Conclusion: Our preclinical proof-of-concept study demonstrated the potential of ¹⁸F-AzaFol as a novel imaging tool for the visualization of macrophage-driven fibrotic lung diseases.

Keywords: interstitial lung disease, imaging biomarkers, animal model of lung fibrosis, macrophages, folate receptor, positron emission tomography, inflammation, folate-based ¹⁸F-PET tracer

INTRODUCTION

In the US, 45% of deaths can be attributed to fibrotic disorders including pulmonary fibrosis (1), for which a global rise in mortality is observed (2). This large and heterogeneous group of parenchymal lung disorders, termed interstitial lung disease (ILD) shares the common feature of pulmonary fibrosis resulting in impaired respiratory function and often failure. The most prevalent forms of ILD are idiopathic pulmonary fibrosis (IPF) and ILD associated with connective tissue diseases (CTD-ILD). CTDs commonly complicated by ILD include systemic sclerosis (SSc) (3), idiopathic inflammatory myopathies (4), rheumatoid arthritis (5), systemic lupus erythematosus (6), Sjögren's syndrome (7), mixed connective tissue disease (8), and undifferentiated connective tissue disease (9). Among the different CTD-ILDs, ILD is most prevalent in SSc with 70–90% of SSc patients developing ILD (10). The life expectancy is markedly reduced, especially in IPF and SSc-ILD, with a median survival of 2–3 years from diagnosis (2, 10).

Despite their clinical heterogeneity, increasing data suggest that in ILD fibrosis develops due to the same dysregulation of wound-healing mechanisms (11, 12). Whereas cell death of alveolar epithelial cells is considered the key trigger of ILD (13, 14), a growing body of (pre-)clinical data point to a similarly crucial pathogenic role of pulmonary macrophages and macrophage-released factors (15, 16). Macrophage activation was shown throughout different stages of ILD including early/mild (17), intermediate (18) as well as end-stage/severe stages (19), and also in different ILD etiologies (20). These observations argue either for a persistent role of macrophages throughout the disease process or for the existence of “inflammatory” or “macrophage-driven” subtypes of ILD (21, 22). Importantly, the persistence of macrophages seems to correlate with poor prognosis and

reduced overall survival (17, 23). Thus, the development of macrophage-targeted imaging techniques for prognostic and treatment purposes in ILD might represent a valuable approach to improve the deleterious disease outcome (15).

Molecular imaging, including nuclear imaging approaches such as positron emission tomography (PET) are sensitive and allow the non-invasive visualization of pathophysiologic processes in real-time. This is a unique advantage over conventional morphological imaging modalities such as high resolution computed tomography (HRCT) scans or magnetic resonance imaging (MRI) (24). These conventional imaging techniques depict anatomical changes in organ architecture with high spatial resolution. They can, however, neither provide information on whether the observed changes are signs of inactive or active tissue remodeling, nor discriminate inflammatory from fibrotic processes, a crucial information for informed clinical decision making (12, 25). An example is the presence of ground glass opacities, which commonly are considered to reflect alveolitis. However, the notion of alveolitis being synonymous to inflammation has been abandoned in fibrosing ILD, since early fibrotic interstitial changes have the same appearance on HRCT (26).

In recent years, several studies have investigated the potential of 2-deoxy-2-¹⁸F]fluoro-D-glucose [¹⁸F]FDG-PET/CT for diagnosis of ILD. [¹⁸F]FDG is an unspecific, metabolic radiotracer for the assessment of cellular glucose metabolism, which has been shown to be elevated in ILD (27, 28). A disadvantage for its use in diagnosis and monitoring of ILD is that [¹⁸F]FDG signals reflect metabolic activity, which can arise from both inflammatory and fibrotic cell types and can occur during different disease stages including those of stabilization or repair. This lacking discrimination of pathophysiologic stages of ILD diminishes the value of [¹⁸F]FDG-PET/CT for informed treatment decisions and monitoring of therapeutic responses (29, 30).

In contrast, imaging approaches using target-specific radiotracers ideally aiming at a single key cell type in ILD may overcome this limitation of [¹⁸F]FDG-PET/CT. So far, only few approaches have been successfully applied pre-clinically in ILD (31–36).

Activated macrophages express folate receptor-β (FR-β) in various pathological conditions including cancer and inflammatory diseases (37–39), whereas the number of FR-β-expressing macrophages is very low under physiological conditions (37, 40).

FR-β is a glycosylphosphatidylinositol (GPI)-anchored protein, which binds folic acid and folate-linked molecules with high affinity and internalizes them via endocytosis. Imaging

Abbreviations: ILD, Interstitial lung disease; PET/CT, Positron emission computed tomography/computed tomography; BLM, Bleomycin; IPF, Idiopathic pulmonary fibrosis; CTD-ILD, Connective tissue disease-associated interstitial lung disease; SSc, Systemic sclerosis; HRCT, High resolution computed tomography; MRI, Magnetic resonance imaging; [¹⁸F]FDG, [¹⁸F]fluorodeoxyglucose; FR-β, Folate receptor-β; GPI, Glycosylphosphatidylinositol; ¹⁸F-AzaFol, 3'-Aza-2'-[¹⁸F]-fluorofolic acid; RT, Room temperature; HE, Hematoxylin and eosin; IHC, Immunohistochemistry; DAB, Diaminobenzidine; AEC, 3-Amino-9-ethylcarbazole; IF, Immunofluorescence; DAPI, 4',6-Diamidino-2-phenylindole; RT-qPCR, Quantitative reverse transcription polymerase chain reaction; mRNA, Messenger RNA; Rplp0, 60S acidic ribosomal protein P0; p.i., Post injection; % IA/g, Percentage of the injected activity per gram of tissue mass; % IA/organ, Percentage of the injected activity per organ; MLEM, Maximum-likelihood expectation maximization IQR, Interquartile range; S.D., Standard deviation; UIP, Usual interstitial pneumonia; NSIP, Non-specific interstitial pneumonia; HP, Hydroxyproline.

of FR- β can be realized with folate radiotracers. A number of folic acid-based radiotracers have been used pre-clinically for the imaging of activated macrophages in non-pulmonary, inflammatory conditions including e.g., rheumatoid arthritis, activated osteoarthritis, or atherosclerosis (41–47), FR-targeted radiopharmaceuticals have, however, not been evaluated yet in the context of ILD. Furthermore, the number of clinical studies making use of FR-targeting nuclear imaging strategies is limited including one exploratory trial in rheumatoid arthritis patients (48), since no folate-based radiotracer for PET imaging is currently available for clinical application.

A novel ¹⁸F-based folate PET radiotracer 3'-Aza-2'-[¹⁸F]-fluoro-folic acid, herein referred to as ¹⁸F-AzaFol, has recently been developed at the Center for Radiopharmaceutical Sciences ETH-PSI-USZ for FR imaging. The rationale to test this radiotracer instead of previously investigated macrophage imaging markers such as translocator protein (TSPO) was based on several disadvantages compared with ¹⁸F-AzaFol: TSPO (a) is mainly expressed in the outer mitochondrial membrane (49), thus it is not a cell surface receptor, (b) exhibits a high multicellular, basal expression in the lungs (50), and (c) TSPO-targeting PET tracers are still facing difficulties for clinical implementation. While the first generation of TSPO PET tracers showed high non-specific binding due to their lipophilic character (51), newer TSPO targeted radiotracers with improved binding specificity and affinity have still limitations due to the allelic dependency of the binding capability resulting from TSPO polymorphisms (52–54).

In this preclinical proof-of-concept study, we aimed to evaluate the potential of ¹⁸F-AzaFol-PET/CT for the specific visualization of macrophage-driven pathophysiologic processes in experimental ILD.

METHODS

Human Subjects

Surgical lung biopsies from patients with IPF ($n = 39$) and CTD-ILD ($n = 14$), who underwent lung transplantation, were analyzed for the expression of FR- β . Lung sections from excess tissue from lung organ donors served as controls ($n = 26$). The patients' characteristics including demographic and clinical data are summarized in the data supplement (**Supplementary Table 1**).

The local ethics committee approved the study (BASEC-No. 2017-01298), and informed consent was obtained from all patients.

Murine Model of Bleomycin-Induced Lung Fibrosis

As a representative animal model for experimental ILD, we used the well-established mouse model of BLM-induced lung fibrosis in this study. In the BLM model, inflammation peaks around day 7, whereas fibrosis reaches its maximum between days 14–21 (33, 35, 55). M1-like macrophages dominate the early inflammatory phase, whereas M2-like macrophages are most abundant in the pro-fibrotic phase, although they might appear as early as day 7 (56, 57).

Female C57BL/6J-rj mice (5–7 weeks old) were purchased from Janvier (Le Genest-Saint-Isle, France) and housed at the institutional animal facilities under defined temperature, humidity, and light conditions, and received *ad libitum* a standard rodent diet. After an acclimatization period of at least 7 days, lung fibrosis was induced in 8-week-old mice by instilling intratracheally a single dose of bleomycin sulfate (4 U/kg of body weight, Baxter, cantonal pharmacy Zurich, Switzerland) dissolved in sterile saline solution under isoflurane anesthesia (33–35). Control mice received equivalent volumes of 0.9% NaCl (50 μ l). At days 3, 7, and 14 after the BLM instillation, biodistribution, and imaging studies were performed. Perfused lungs of separate animals were harvested for immunostainings, histological, and molecular analyses.

All animal experiments performed in this study were approved by the cantonal veterinary offices and conducted in strict compliance with the Swiss animal welfare guidelines. For all experiments, mice were randomized into the different study groups in a non-blinded manner.

Histology

For histology, perfused middle, caudal, and accessory lobes of the right mouse lung were inflated with 10% neutral-buffered formalin solution and fixed overnight at room temperature (RT). After embedding in paraffin, lung sections were cut at a thickness of 4 μ m and stained with hematoxylin and eosin (HE) for analysis of the lung architecture and the presence of cellular infiltrates, and with Picrosirius Red to detect collagen deposition using standard protocols.

Immunohistochemistry on Murine Lung Tissues

For immunohistochemistry (IHC) on murine tissues, lung sections were deparaffinized and rehydrated, and then subjected to heat-mediated antigen retrieval with 10 mM sodium citrate buffer (pH = 6.0) at 95°C for 15 min. After blocking of endogenous peroxidase activity with 3% hydrogen peroxide (15 min, RT), sections were blocked with 10% normal goat serum (1 h, RT) followed by blocking of endogenous biotin using an Avidin/Biotin blocking kit (Vector Laboratories, Burlingame, CA, United States). Afterwards, primary antibodies for F4/80 (rat anti-mouse F4/80, clone Cl:A3-1, 1:100, AbD Serotec; Kidlington, United Kingdom), and FR- β (rabbit anti-mouse FR- β , 1:400, Genetex, Irvine, CA, United States) were applied on the specimens and incubated overnight at 4°C. Isotype- and concentration-matched IgGs served as negative controls. Next, biotin-labeled goat anti-rat or anti-rabbit secondary antibodies (all from Vector Laboratories) were applied (30 min, RT). This was followed by incubation with the Vectastain ABC Elite HRP kit for 30 min at RT (Vector Laboratories). Finally, stainings were visualized using 3,3'-diaminobenzidine (DAB) in case of F4/80, or 3-amino-9-ethylcarbazole (AEC) (all from Vector Laboratories) in case of FR- β , and sections were counterstained with Mayer's hematoxylin (J.T. Baker, Deventer, Netherlands).

Immunohistochemistry on Human Lung Tissues

Immunohistochemistry was performed using an automated single-staining procedure (Benchmark Ultra; Ventana Medical Systems). Briefly, 4 μm thick sections were stained using mouse monoclonal anti-human antibodies directed against CD68 (clone PG-M1, Dako, 1:50) and FR-β (clone OTI8G1, Origen, 1:50). Detection was completed with respective secondary antibodies and the OptiView DAB Kit (Ventana Medical Systems).

Immunofluorescence

Immunofluorescence (IF) stainings were performed using the MaxDouble IF staining kits for rat and rabbit primary antibodies (MaxVision Biosciences Inc., Bothell, WA, United States). In brief, after blocking of auto-fluorescence for 5 min at RT, heat-mediated antigen retrieval with 10 mM sodium citrate buffer was performed for 15 min at 95°C. After antigen retrieval, primary antibodies for FR-β (rabbit anti-mouse FR-β, 1:800, Genetex), and F4/80 (rat anti-mouse F4/80, clone Cl:A3-1, 1:800, AbD Serotec), or concentration matched IgG isotype controls were applied and incubated overnight at 4°C. Next, specimens were incubated with rat and rabbit signal amplifier for 30 min at RT followed by washing and linkage to the respective fluorophores for 60 min at RT in the dark (anti-rat MaxFluor488 and anti-rabbit MaxFluor594). Cell nuclei were counterstained with 4',6-diamidino-2-phenylindole (DAPI).

Microscopy and Image Analysis

Histological and immunohistochemical stainings were recorded automatically with the AxioScan.Z1. slidescanner (Carl Zeiss, Feldbach, Switzerland) using a Plan-Apochromat 20×/0.8 M27 objective. For semi-quantitative expression analyses, per sample, six randomly selected high power fields were extracted with a 10× objective using the *Zen 2.0 lite* (blue edition) software. The percentage of positively stained pixels was automatically quantified using an in-house designed *MATLAB* script (Mathworks, *MATLAB* R2016b) to avoid observer bias. This script quantified the target-positive (=brown or red) pixels and cell nuclei-positive (=blue) pixels and calculated the percentage of positively stained pixels in relation to the total number of image pixels. To account for increased cell numbers and tissue consolidations, also the percentage of positively stained pixels in relation to the total number of colored image (brown or red + blue) pixels was calculated (**Supplementary Figure 1**).

For semi-quantitative assessment of murine and human lung fibrosis, the Ashcroft Score was applied on Picrosirius Red stained lung sections as described previously (58). Two blinded examiners performed the scorings in duplicates. If deviations of more than 1 score were observed, the respective slides were re-assessed to reach consensus.

Immunofluorescent pictures were recorded at 630× magnification (oil immersion) using the Olympus BX53 microscope in fluorescence mode (Olympus, Volketswil, Switzerland).

The total number of double positive (FR-β+/F4/80+) cells was quantified by both automated and manual image analyses

using Orbit image analyses software version 3.15 (Objection Detection and Object Classification Module) (59) or manual counting by two blinded examiners, respectively.

RNA Extraction and Quantitative Reverse Transcription PCR

For RNA extraction from mouse lungs, perfused cranial lobes were homogenized using the Qiagen TissueLyser and total RNA was isolated with the RNeasy Fibrous Tissue Mini Kit from Qiagen (Hombrechtikon, Switzerland). For quantitative reverse transcription PCR (RT-qPCR), 120 ng RNA were reverse-transcribed into complementary DNA with the Transcriptor First Strand cDNA Synthesis Kit from Roche (Basel, Switzerland) using anchored-oligo(dT)₁₈ primer. Messenger RNA (mRNA) expressions were analyzed by SYBR Green qPCR on a Stratagene Mx3005P qPCR System (Agilent Technologies, Santa Clara, California, USA) using the SYBR Green GoTaq qPCR Master mix from Promega (Dübendorf, Switzerland) and specific primers for murine *Folr2* (forward primer: 5'-CCAGCAAGTGGACCA GAGTT-3', reverse primer: 5'-CAGTCCCAGCCTTTATGCCA-3'; Microsynth, Balgach, Switzerland). As a housekeeping gene 60S acidic ribosomal protein P0 (*Rplp0*; forward primer: 5'-GCAGGTGTTTGACAACGGCAG-3', reverse primer: 5'-GAT GATGGAGTGTGGACCGA-3'; Microsynth) was used. The fold change of mRNA expression was calculated using the $2^{-\Delta\Delta Ct}$ method. False positive results due to primer dimers or genomic contamination were excluded by dissociation curve analysis and non-template controls, or by minus-reverse transcriptase controls, respectively.

Hydroxyproline Assay

Collagen contents in lungs of BLM-treated mice and saline controls were quantified by hydroxyproline assay as described previously (60). Briefly, after homogenization, left lung lobes were digested in 6 M HCl for 3 h at 120°C and subsequently neutralized with 6 M NaOH. Next, samples were mixed with a 60 mM chloramine T solution and incubated for 20 min at RT. After addition of 3.15 M perchloric acid (5 min, RT), p-Dimethylaminobenzaldehyd (20% w/v) was added and samples were incubated for 20 min at 60°C. The absorbance was measured at 560 nm with a spectrophotometer (*GloMax-Multi Detection System*, Promega, Dübendorf, Switzerland).

Radiosynthesis of ¹⁸F-AzaFol

3'-Aza-2'-[¹⁸F]-fluoro-folic acid (¹⁸F-AzaFol) was produced on an automated synthesis module at the ETH Zurich (Switzerland) according to a previously reported method (61). ¹⁸F-AzaFol was applied at ~5 MBq (in 100 μL, 0.25–0.5 pmol/mouse) for biodistribution studies and at ~10 MBq (in 100 μL, 0.5–1 pmol/mouse) for *in vivo* and *ex vivo* PET/CT imaging. The *in vivo* stability of the tracer has been demonstrated in previous studies, in which only the intact parent radiotracer was detected. No downstream radiometabolites in blood plasma, urine, or liver samples were detectable (61, 62).

TABLE 1 | Scan parameters for *in vivo* and *ex vivo* PET scans using G8 bench-top PET/CT scanner.

Energy window	150–650 keV
Isotope	Fluorine 18
Framing sequence	Static
Duration of static PET scans	
<i>In vivo</i> (chest region)	10 min
<i>Ex vivo</i> (isolated whole lungs)	20 min
Normalization	Yes
Dead time correction	Yes
Decay correction	Yes
Scatter correction	No
Image reconstruction	
Number of iterations	60
Attenuation correction	Yes

In vivo and *ex vivo* scans were performed 1 h after the injection of ¹⁸F-AzaFol (~10 MBq in 100 μL, 0.5–1 pmol/per mouse).

Biodistribution Studies

As an accurate means to quantify radiotracer uptake (31), biodistribution studies were performed. ¹⁸F-AzaFol was administered via the lateral tail vein of mice. Receptor-blocking studies were performed by pre-injection of folic acid (leucovorin; 300 nmol, 100 μL) ~30 min before the injection of ¹⁸F-AzaFol. Mice were sacrificed 1 h post injection (p.i.) of ¹⁸F-AzaFol. Tissues and organs of interest were collected, weighed and counted for activity using a γ-counter (Wallac Wizard 1480, Perkin Elmer, Germany). The results were calculated as a percentage of the injected activity per gram of tissue mass (% IA/g) or expressed as a percentage of the injected activity per organ (% IA/organ). Thereafter, the already counted lungs were subjected to *ex vivo* PET/CT scans as described below.

Ex vivo and *in vivo* PET/CT Scans

The *ex vivo* PET/CT scans of collected lungs (obtained from mice used for the biodistribution study) were performed using a small-animal bench-top PET/CT scanner (G8, Perkin Elmer, Massachusetts, USA; **Table 1**). Static PET scans of 20 min duration were acquired using the G8 acquisition software (version 2.0.0.10) followed by CT scans of 1.5 min duration. The energy window ranged from 150 to 650 keV. The PET data were corrected for random coincidences, decay, and dead time and reconstructed with maximum-likelihood expectation maximization (MLEM). A correction for scatter was not made. The images were prepared using VivoQuant post-processing software (version 3.0, inviCRO Imaging Services and Software, Boston, USA). A Gauss post-reconstruction filter (FWHM = 1 mm) was applied to the PET images. The *ex vivo* PET/CT scans and biodistribution studies were performed in a separate experiment as the *in vivo* PET/CT scans. For *in vivo* imaging, static PET scans were performed 1 h p.i. of the radiotracer and lasted for 10 min followed by a CT of 1.5 min duration. During the *in vivo* PET/CT scans, the mice were anesthetized with a mixture of isoflurane and oxygen. The *in vivo* images were visualized using a dedicated 3D-rendering software (Ziostation2, Ziosoft, Tokyo, Japan).

For both, biodistribution studies/*ex vivo* scans and the *in vivo* scans per each time point the following numbers of mice have been used: $n = 3–4$ for saline-treated mice, $n = 3–4$ for BLM-treated mice and $n = 2–4$ for BLM-treated mice receiving leucovorin for FR blockade.

Statistics

Statistical analysis was performed using GraphPad Prism 7 software (version 7.04). Unless otherwise indicated, non-parametric data were expressed as median ± interquartile range (IQR) and parametric data were expressed as mean ± standard deviation (S.D.). For non-parametric non-related data, the Mann–Whitney *U*-test for comparison of two groups, or the Kruskal–Wallis test followed by Dunn's multiple correction for comparison of multiple groups was employed. For parametric non-related data, an unpaired *t*-test was applied for comparison between two groups, or a One-Way ANOVA with Tukey's *post-hoc* test for comparison between multiple groups was performed. For correlation analysis, Spearman rank correlation was performed. *P*-values < 0.05 were considered statistically significant.

RESULTS

FR-β Expression Is Upregulated in Human ILD and Correlates With Disease Severity

To assess the presence of FR-β-positive macrophages in human ILD, we performed IHC for FR-β on lung explants derived from patients with IPF ($n = 39$) and CTD-ILD ($n = 14$), who underwent lung transplantation. Lung sections from excess tissue from lung organ donors served as controls ($n = 26$) (**Supplementary Table 1**).

As anticipated, the histopathological analysis of lung tissues from both patients with IPF and CTD-ILD revealed severe damage of the normal tissue architecture with increased numbers of mononuclear inflammatory infiltrates and excessive interstitial collagen deposition as assessed by HE or Picrosirius Red staining (**Figure 1A**), respectively. This was also reflected in the semi-quantitative Ashcroft score of pulmonary fibrosis with a median score of 6.125 (Q1, Q3 = 5.625, 6.5; $p < 0.0001$) for IPF and a median score of 5 (Q1, Q3 = 4.219, 6.531; $p < 0.0001$) for CTD-ILD patients (**Figure 1B**). In most cases, lung remodeling in IPF and CTD-ILD patients had histological features of usual interstitial pneumonia (UIP) characterized by patchy fibrosis and areas of honeycombing, whereas only the minority of patients displayed patterns of non-specific interstitial pneumonia (NSIP), characterized by a more uniformly spread fibrosis and better preserved lung architecture (**Supplementary Table 1**). In these highly inflammatory and fibrotic lung sections, presence of FR-β was significantly increased (**Figure 1A**) with median increases of ~ 3- to 4-fold in both IPF and CTD-ILD patients (**Figure 1C, Supplementary Figure 2A**; $p < 0.0001$). To confirm the expression of FR-β on macrophages (40, 63), we additionally performed IHC for CD68, a human pan-macrophage marker, on sequential lung sections from healthy controls, IPF and CTD-ILD patients. In accordance with the increased FR-β expression, we also found increased CD68 expression in lung sections

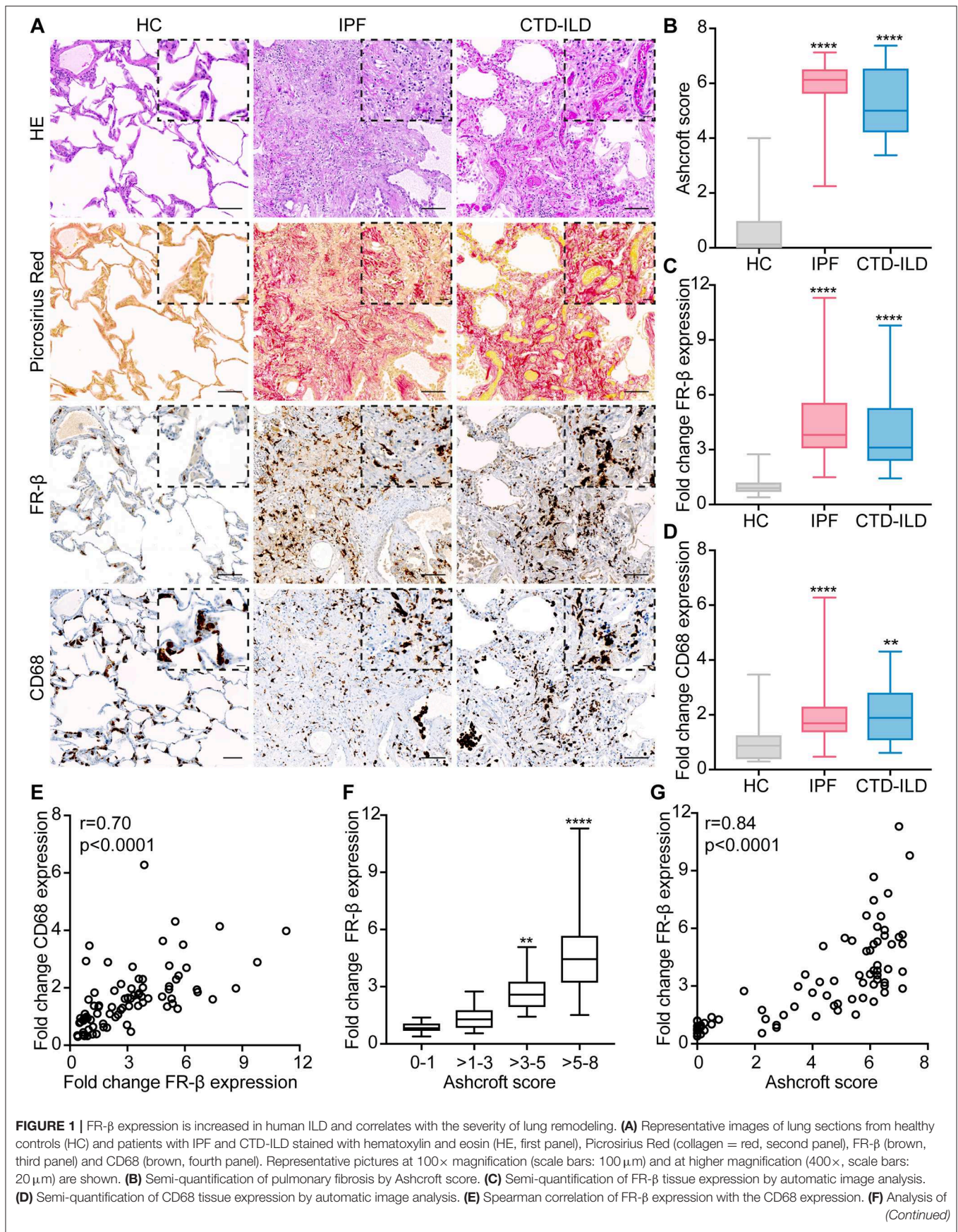


FIGURE 1 | FR- β expression according to the severity of lung remodeling as defined by the Ashcroft score (score 0–1: no fibrosis, scores >1–3: mild fibrosis, scores >3–5: moderate fibrosis, scores >5–8: severe fibrosis). **(G)** Spearman correlation of FR- β expression with the Ashcroft score. For **(B–D,F)** data are displayed as box plots with min/max values. For statistical analysis, the Kruskal–Wallis test with Dunn's multiple correction was applied (* $p < 0.05$, ** $p < 0.01$, *** $p < 0.001$, **** $p < 0.0001$). For all experiments: $n = 26$ for healthy controls, $n = 39$ for IPF patients, and $n = 14$ for CTD-ILD patients.

from both IPF and CTD-ILD patients with median increases of 1.69-fold (Q1, Q3 = 1.37, 2.29; $p < 0.0001$) and 1.89-fold (Q1, Q3 = 1.09, 2.8; $p < 0.01$), respectively (**Figure 1D**, **Supplementary Figure 2B**). Consistently, FR- β expression also strongly correlated with the CD68 expression ($r = 0.70$, $p < 0.0001$; **Figure 1E**). Whereas, a strong expression of CD68 was observed on macrophages in the alveolar spaces, FR- β was mostly expressed in the lung interstitium (**Figure 2**). Furthermore, while the upregulation of CD68 and FR- β in IPF and CTD-ILD patients was independent of the histological subtype (**Supplementary Figure 3**), the expression of FR- β significantly increased with the severity of lung remodeling (**Figure 1F**) and positively correlated with the Ashcroft score as measure of lung remodeling ($r = 0.84$, $p < 0.0001$; **Figure 1G**).

FR- β Expression Is Also Upregulated in Experimental ILD and Changes With Disease Development

Next, we assessed whether the expression of FR- β was mirrored in a representative mouse model of human ILD, the BLM-induced lung fibrosis model.

Upon a single intratracheal BLM administration, mice progressively developed lung remodeling with inflammation (days 3–7) preceding the development of pulmonary fibrosis (day 14). As early as day 3, the histopathological examination of lung sections from BLM-treated mice vs. saline controls revealed the presence of mononuclear cell infiltrates (**Figure 3A**) around the vessels and bronchi with increased numbers of macrophages as assessed by IHC with the murine macrophage marker F4/80 (**Figure 3B**). In contrast, only minimal fibrous thickening of the alveolar and bronchial walls (**Figure 3C**) was detected, which was also reflected by a low median Ashcroft score of 2.5 (Q1, Q3 = 2, 3; $p < 0.01$; **Figure 3D**). With disease progression, the number of macrophages increased in BLM-treated lungs and peaked at day 7 with a median 4.11-fold increase (Q1, Q3 = 2.38, 10.65; $p < 0.001$; **Figure 3E**, **Supplementary Figure 2D**) and subsided thereafter. Consistently, pulmonary fibrosis gradually increased with extensive interstitial collagen deposition characterized by the formation of fibrous bands and larger fibrous masses in subpleural as well as perivascular and peribronchial areas (**Figure 3C**). Maximally established fibrosis was detected at day 14 as demonstrated by a high median Ashcroft score of 5 (Q1, Q3 = 4.25, 5.5; $p < 0.001$). The lung collagen content as assessed by hydroxyproline (HP) assay increased over time in BLM-treated mice with a median 1.32-fold (Q1, Q3 = 1.17, 1.42; $p < 0.05$) increase at day 14 (**Figure 3F**).

In accordance with the expression in human ILD and the time course of the appearance of pulmonary macrophages in this animal model, FR- β expression significantly increased

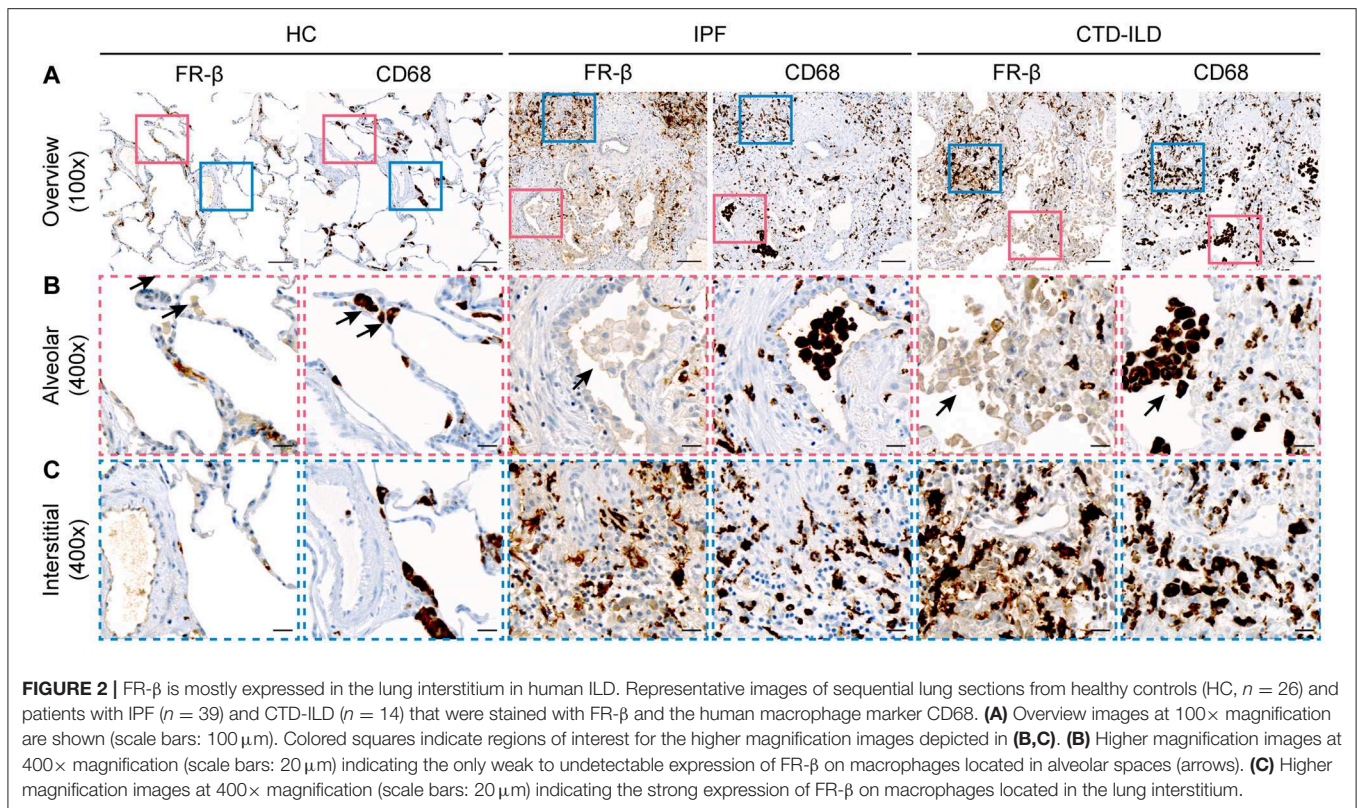
over time in lungs of BLM-treated mice (**Figure 4A**). While FR- β was only weakly expressed in the lungs of saline-treated controls, FR- β expression was significantly upregulated in lungs of BLM-treated mice with peak at day 3 at the mRNA level (**Figure 4B**) and at day 7 at the protein level (**Figures 4A,C**, **Supplementary Figure 2C**) and thus in the inflammatory phase in this animal model with a median increase of 1.98-fold (Q1, Q3 = 1.61, 2.19; $p < 0.001$) and 4.41-fold (Q1, Q3 = 2.4, 6.83; $p < 0.01$), respectively. The expression of FR- β on murine lung macrophages was confirmed by immunofluorescent double staining using an antibody for murine macrophages, F4/80 (**Figure 4D**, **Supplementary Figure 4**).

As in human ILD patients, the expression of FR- β also positively correlated with the Ashcroft score ($r = 0.64$, $p < 0.0001$; **Figure 4E**) and, hence, with the degree of lung remodeling (**Figure 4F**).

Pulmonary Accumulation of ¹⁸F-AzaFol, a Surrogate Marker for FR- β -Positive Macrophages, Reflects Macrophage-Related Disease Development in Experimental ILD

Having established the time course of FR- β expression in this mouse model, we next performed nuclear imaging experiments to assess whether macrophage-related disease development could be visualized by ¹⁸F-AzaFol.

In strong correlation with the expression changes of FR- β at the tissue level, BLM-treated mice showed increased pulmonary accumulation of ¹⁸F-AzaFol from days 3 to 14, as assessed by *ex vivo* biodistribution studies at 1 h p.i. of ¹⁸F-AzaFol (**Figures 5A,B**). The maximum lung accumulation was observed at day 7 with a mean total uptake of $1.01 \pm 0.30\%$ injected activity per lung (% IA/lung) and $3.33 \pm 0.77\%$ injected activity per tissue mass (% IA/g) in BLM-treated vs. control animals ($0.31 \pm 0.06\%$ IA/lung and $1.78 \pm 0.15\%$ IA/g; $p < 0.01$ and $p < 0.05$, respectively). The specificity of the pulmonary tissue uptake of ¹⁸F-AzaFol was validated by receptor blockade using folinic acid (leucovorin) administered to mice 30 min prior to the injection of the radiotracer. This significantly reduced the lung accumulation of ¹⁸F-AzaFol in BLM-treated mice, resulting in pulmonary radioactivity accumulation comparable to saline-treated controls. *Ex vivo* PET/CT scans of isolated lungs also clearly distinguished diseased from healthy lungs and confirmed the successful receptor blockade (**Figure 5C**). *In vivo* PET/CT scans of the chest region of the animal showed a generally low pulmonary accumulation of ¹⁸F-AzaFol with background signals in bone and muscles in both NaCl-treated controls and BLM-treated mice. A slightly increased signal intensity compared with control mice was observed in lungs of BLM-treated mice at the maximum of inflammation at day 7 (**Supplementary Figure 5**).



The distribution of ^{18}F -AzaFol in other organs besides the lungs was comparable between BLM-treated mice and saline-treated control animals at day 7 (**Figure 5D**, **Supplementary Tables 2, 3**). The slightly increased uptake in both experimental groups in lymphoid organs (e.g., thymus, lymph nodes), which may have been also affected by the BLM treatment (64), is most likely caused by the presence of activated macrophages expressing FR- β (65, 66), a phenomenon, previously observed in lymph nodes of tumor-bearing mice (61). The high basal liver uptake of ^{18}F -AzaFol observed in both controls and BLM-treated mice can be explained by the fact that folate vitamins are physiologically stored in the liver. Since ^{18}F -AzaFol is not a conjugate of folic acid, as this is the case with other folate radioligands, ^{18}F -AzaFol may also be transported through carrier systems such as the proton-coupled folate transporter. A relatively high liver uptake and potential signs of metabolism were also shown in our previous studies, in which we evaluated ^{18}F -AzaFol for the first time (61).

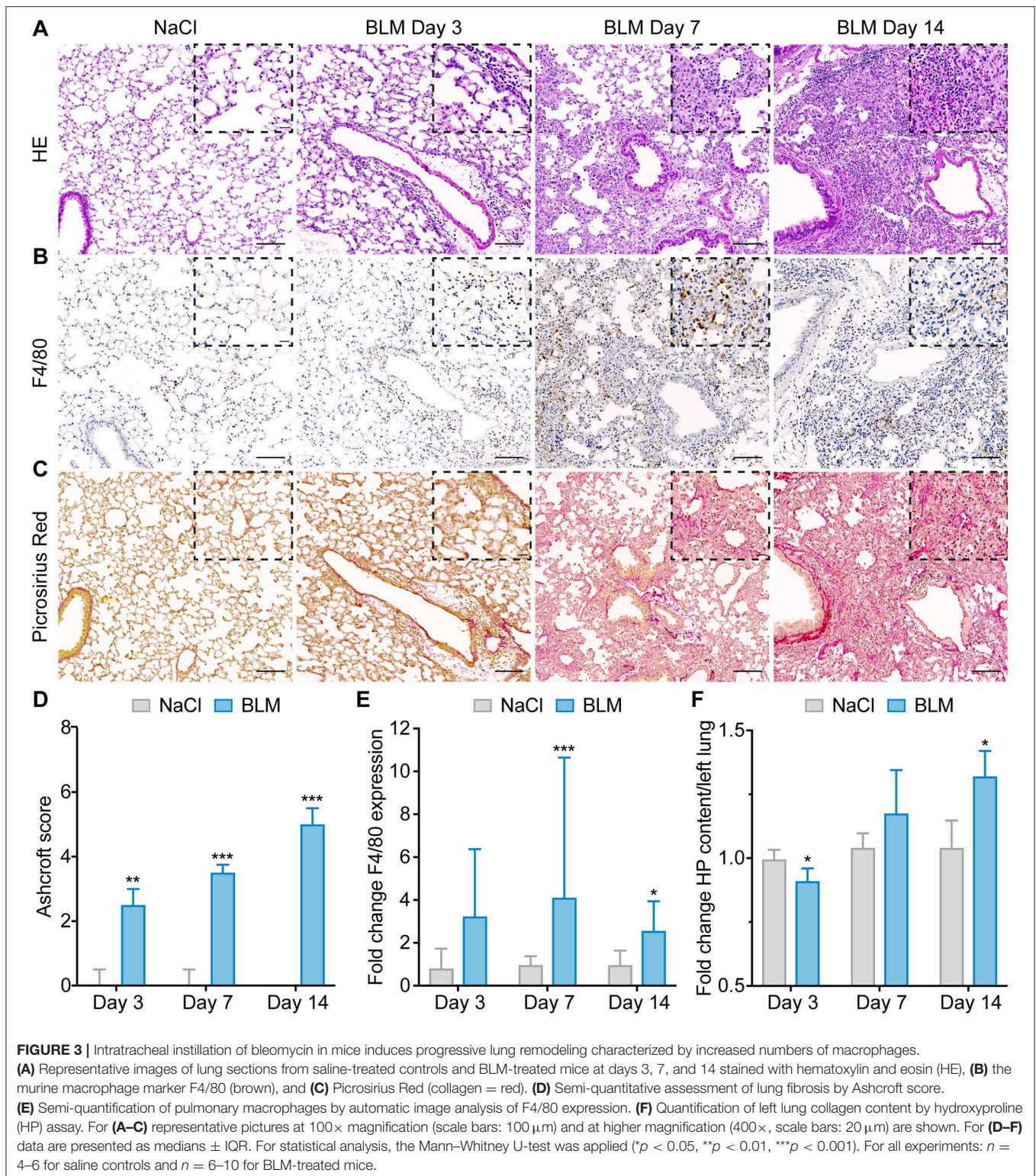
The distinct drop in activity after treatment with the FR blocking agent in both liver and lymph nodes further argues for a folate-specific effect rather than an unspecific accumulation mechanism.

DISCUSSION

In different types of ILD, an increased lung uptake of [^{18}F]FDG was observed in pathologically changed areas of reticulation/honeycombing and ground-glass opacities, but also

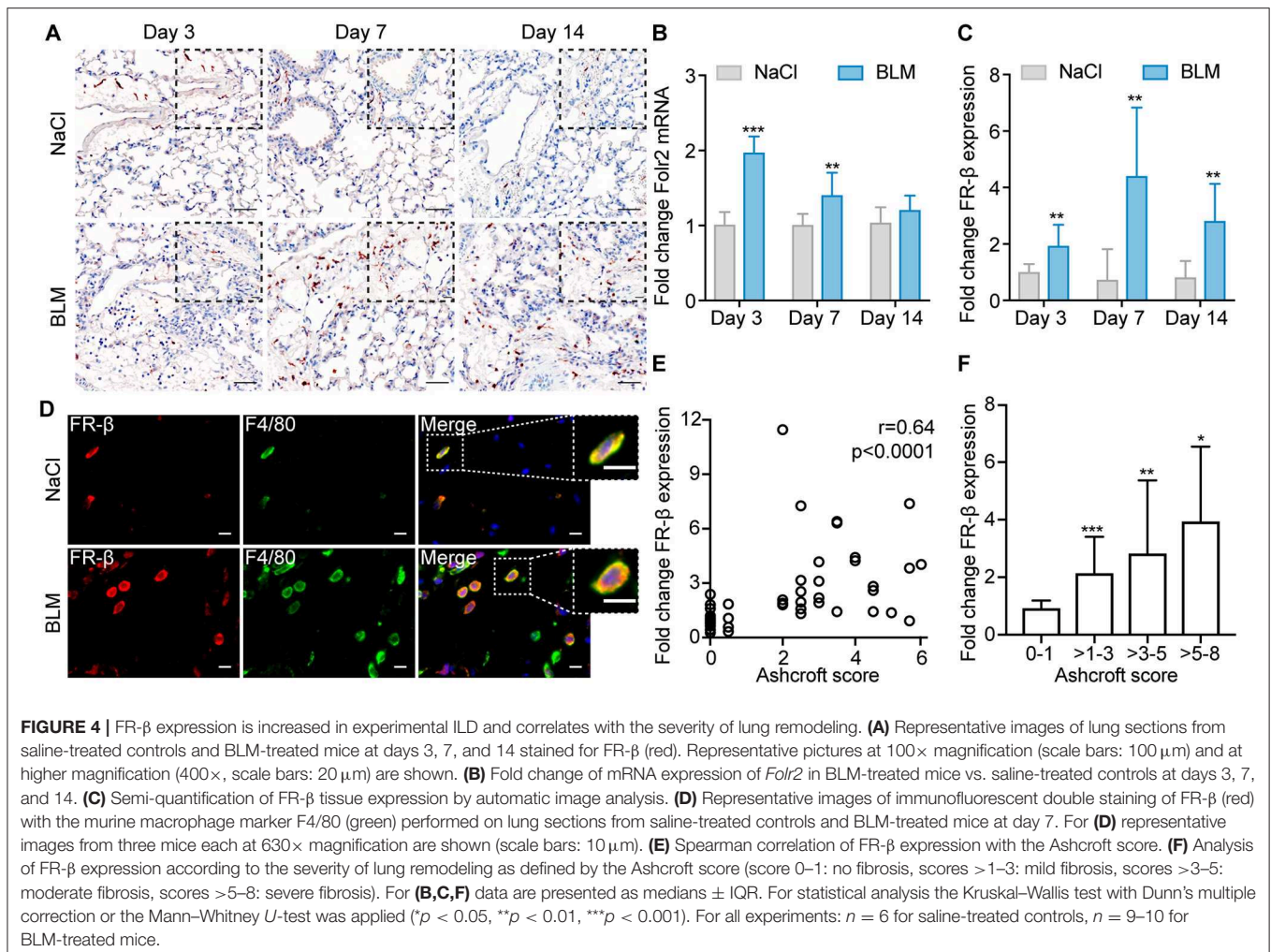
in radiologically normal-appearing lung areas (28, 29, 67–71). [^{18}F]FDG uptake, especially in normal appearing lung parenchyma, was shown to be of prognostic value and to correlate with overall disease severity in IPF patients (28, 68, 70). However, [^{18}F]FDG-PET/CT has also important limitations for the diagnosis and monitoring of ILD since it visualizes changes in glucose metabolism in a non-specific, cell-type-independent manner (25, 26, 67), and does not allow to draw conclusions on the pathophysiological disease stage (30, 72). In our study, ^{18}F -AzaFol visualized macrophage-related ILD development in the mouse model of BLM-induced lung fibrosis in *ex vivo* PET/CT scans and tissue expression of FR- β showed good correlation with the pulmonary radiotracer uptake in the biodistribution studies. This has important clinical implications.

As ILDs are highly heterogeneous on molecular level, such a targeted molecular imaging approach could be used in the future for a molecular stratification of ILD patients, i.e., the identification of subgroups of patients, who are likely to benefit from macrophage-oriented therapies and who will be eligible for subsequent monitoring of therapeutic responses. This is of particular interest due to the recent or imminent approval of such therapies for ILD (73–75). These include pirfenidone and nintedanib, which have pre-clinically shown to exert their anti-fibrotic effects at least partially by targeting pulmonary macrophages and/or their products (75–77) as well as tocilizumab, which was assessed in recent phase II and III randomized controlled studies (78). In addition, the ability to identify ILD patients based



on their underlying molecular and cellular subtype without the need of lung biopsies might also have relevance for clinical trial design by allowing the definition of (more) homogenous patients' subgroups and by serving as a primary/secondary readout for macrophage-orientated

treatment studies. To this end, additional preclinical studies to confirm the suitability for ^{18}F -AzaFol for predicting and monitoring therapeutic efficacy will have to be performed. The alterations of tissue uptake of ^{18}F -AzaFol throughout the development of experimental ILD were in strong accordance

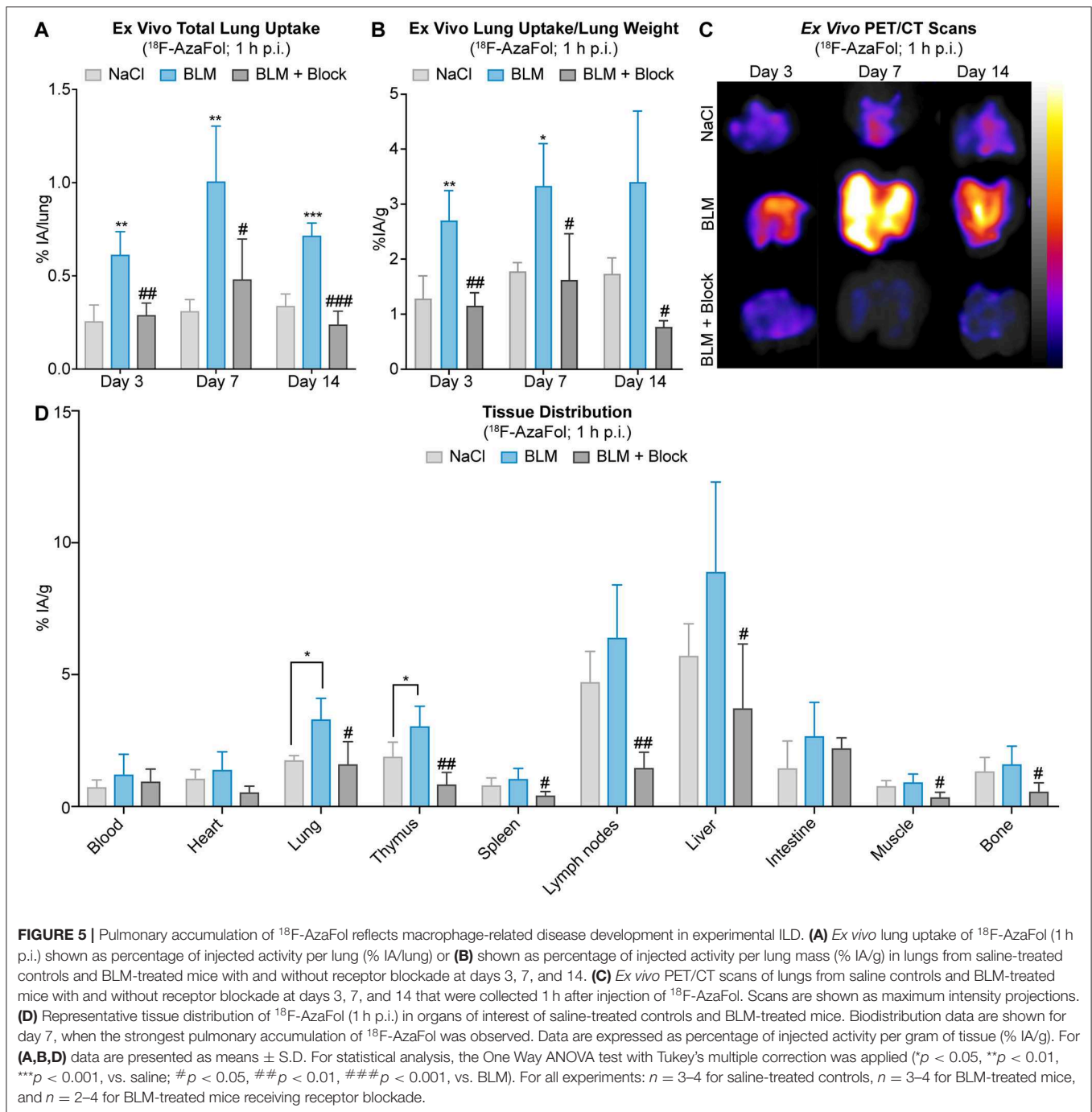


with the time course of macrophage presence on tissue level, which documents a good sensitivity to change. This quality is an important prerequisite for the monitoring of macrophage-targeted treatment responses, which we have not yet tested pre-clinically.

Another important finding of this study was that the numbers of (FR- β -positive) macrophages were substantially increased in human ILD patients, irrespective of the underlying etiology. This observation has some interesting implications. Firstly, it supports the re-evaluation of the pathophysiology of fibrotic ILD as immune-mediated and thus, as potentially amenable to immune-targeted therapies (12). Secondly, the persistence of macrophages throughout different stages of experimental ILD and their presence in late disease stages in the human disease points to an important role in the whole process of tissue remodeling (79). Thus, the characterization of macrophage subpopulations, particularly of FR- β -positive macrophages, might further elucidate the mechanisms of fibrosis in ILD and identify novel macrophage- or macrophage-related therapeutic targets (15) including FR- β -targeted molecular therapies (40, 80–82).

The exploratory character of our study accounts for some of its limitations. The model of BLM-induced lung fibrosis, although extensively used and widely acknowledged as a valuable model of experimental ILD, does not reflect the chronic disease course in human patients, since following the single instillation of BLM, fibrosis gradually resolves over 4–8 weeks (55). Furthermore, the imaging analyses have been limited to the stages of active disease and later time points of resolution of fibrosis (days 21–28) have not been investigated. For pathophysiologic studies to elucidate the whole process of macrophage-related tissue remodeling in ILD in detail, FR- β -targeted nuclear imaging would have to be performed (a) in the phase of tissue repair in the acute BLM model and (b) in non-resolving, chronic disease models of ILD (83). Numerous studies, however, are now focusing on the acute, pro-inflammatory phase and the role of macrophages in fibrosis development in this model (15, 56, 57), which support the importance and comparability of its early stages to certain aspects of human ILD.

Another important limitation of our proof-of-concept study is that our nuclear imaging experiments are largely based on *ex vivo* analyses and quantifications. Furthermore, the performance



of static PET scans did not allow the correction for changes in pulmonary blood flow. Elevated blood flow and increased vascular leakage are cardinal features of lung inflammation and fibrosis (34, 84). These phenomena could have contributed non-specifically to the pulmonary accumulation of ¹⁸F-AzaFol in BLM-treated mice. The fact that receptor blockade with folic acid lowered the radiotracer uptake to the level of control mice, however, points to a receptor-specific rather than a non-specific pulmonary uptake of ¹⁸F-AzaFol.

In future preclinical experiments to further support the specificity of ¹⁸F-AzaFol-PET/CT, (a) the quality of the *in vivo* imaging should be improved by using gated respiration during the acquisition of the nuclear images to reduce motion artifacts, which could affect tissue density, (b) dynamic PET scans should be performed to account for blood flow-related changes, and (c) signal intensities should be also quantified *in vivo* e.g., by calculating the standardized uptake values (84, 85). These additional studies would allow to better

estimate the clinical applicability of ¹⁸F-AzaFol-PET/CT. For the extrapolation of our preclinical data to humans, it is further important to note that the endogenous folate levels largely differ between rodents and humans (~15–40 fold higher in mice). In our study, this could have led to an underestimation of the actual ¹⁸F-AzaFol tissue uptake since endogenous folate might also compete with ¹⁸F-AzaFol for binding to the FR (86).

In general, the transferability of results from animal models, which, even though representative of certain aspects, never cover the whole complexity of a human disease, is always a matter of debate. However, previous studies using the murine BLM-induced lung fibrosis model provided evidence for its suitability for both imaging (33, 87) and molecular analyses (88) and our own data showed similarly high pulmonary expression levels of FR-β in experimental and (end-stage) human ILD.

In conclusion, our proof-of-concept study showed that nuclear imaging using ¹⁸F-AzaFol can visualize macrophage-related experimental ILD. The fact that FR-β—apart from being a cellular rather than a metabolic marker—is only expressed on activated macrophages in disease states such as inflammatory disorders or malignancies, supports ¹⁸F-AzaFol as a more specific alternative to [¹⁸F]FDG in ILD. Since ¹⁸F-AzaFol-PET/CT has been tested for targeting FR-positive tumors in a Swiss multi-center trial (NCT03242993; www.clinicaltrials.gov), its clinical availability, including first-in-human clinical trials for imaging of ILD, is impending.

DATA AVAILABILITY STATEMENT

All datasets generated for this study are included in the article/**Supplementary Material**.

ETHICS STATEMENT

The studies involving human participants were reviewed and approved by Ethics committee Zurich. The patients/participants provided their written informed consent to participate in this study. The animal study was reviewed and approved by Swiss veterinary office. The local ethics committee approved the study

REFERENCES

- Wynn TA. Fibrotic disease and the T(H)1/T(H)2 paradigm. *Nat Rev Immunol.* (2004) 4:583–94. doi: 10.1038/nri1412
- Hutchinson JP, McKeever TM, Fogarty AW, Navaratnam V, Hubbard RB. Increasing global mortality from idiopathic pulmonary fibrosis in the twenty-first century. *Ann Am Thorac Soc.* (2014) 11:1176–85. doi: 10.1513/AnnalsATS.201404-145OC
- Hoffmann-Vold AM, Fretheim H, Halse AK, Seip M, Bitter H, Wallenius M, et al. Tracking impact of interstitial lung disease in systemic sclerosis in a complete nationwide cohort. *Am J Respir Crit Care Med.* (2019). doi: 10.1164/rccm.201903-0486OC
- Long K, Danoff SK. Interstitial lung disease in polymyositis and dermatomyositis. *Clin Chest Med.* (2019) 40:561–72. doi: 10.1016/j.ccm.2019.05.004

(BASECNo. 2017-01298), and informed consent was obtained from all patients.

AUTHOR CONTRIBUTIONS

JS made substantial contributions to the conception of the study and the acquisition, analysis and the interpretation of data, and was involved in drafting and revising the manuscript. MBe, MBr, SH, SC, TF, BV, and CF-B were centrally involved in the acquisition and analysis of data and in revising the manuscript. RS and OD made contributions to the conception and design of the study, the interpretation of the data, and the revision of the manuscript. CM and BM made substantial contributions to conception, design of the study and were centrally involved in the acquisition, analysis and interpretation of data, and in drafting and revising the manuscript.

FUNDING

This work was supported by the Swiss National Science Foundation: grant: CRSII3_154490 and grant: 310030_156803, Hartmann-Mueller Foundation (BM), Swiss Personalized Health Network Grant 2017DRI09 (OD), Prof. Max Cloetta Foundation (BM), and by the National Institutes of Health grant P30 AR061271 (CF-B).

ACKNOWLEDGMENTS

We thank Maria Comazzi (Center of Experimental Rheumatology, University Hospital Zurich, Switzerland) for her technical assistance and Susanne Geistlich und Annette Krämer for the production of ¹⁸F-AzaFol for this study. Microscopic image recording was performed with equipment maintained by the Center for Microscopy and Image Analysis, University of Zurich.

SUPPLEMENTARY MATERIAL

The Supplementary Material for this article can be found online at: <https://www.frontiersin.org/articles/10.3389/fimmu.2019.02724/full#supplementary-material>

- Brito Y, Glassberg MK, Ascherman DP. Rheumatoid arthritis-associated interstitial lung disease: current concepts. *Curr Rheumatol Rep.* (2017) 19:79. doi: 10.1007/s11926-017-0701-5
- Tselios K, Urowitz MB. Cardiovascular and pulmonary manifestations of systemic lupus erythematosus. *Curr Rheumatol Rev.* (2017) 13:206–18. doi: 10.2174/1573397113666170704102444
- Roca F, Dominique S, Schmidt J, Smail A, Duhaut P, Levesque H, et al. Interstitial lung disease in primary Sjogren's syndrome. *Autoimmun Rev.* (2017) 16:48–54. doi: 10.1016/j.autrev.2016.09.017
- Reiseter S, Gunnarsson R, Mogens Aalokken T, Lund MB, Mynarek G, Corander J, et al. Progression and mortality of interstitial lung disease in mixed connective tissue disease: a long-term observational nationwide cohort study. *Rheumatology.* (2018) 57:255–62. doi: 10.1093/rheumatology/kex077
- Fischer A, Brown KK. Interstitial lung disease in undifferentiated forms of connective tissue disease. *Arthritis Care Res.* (2015) 67:4–11. doi: 10.1002/acr.22394

10. Wallace B, Vummidu D, Khanna D. Management of connective tissue diseases associated interstitial lung disease: a review of the published literature. *Curr Opin Rheumatol.* (2016) 28:236–45. doi: 10.1097/BOR.0000000000000270
11. Maher TM, Wells AU, Laurent GJ. Idiopathic pulmonary fibrosis: multiple causes and multiple mechanisms? *Eur Respir J.* (2007) 30:835–9. doi: 10.1183/09031936.00069307
12. Wells AU, Denton CP. Interstitial lung disease in connective tissue disease—mechanisms and management. *Nat Rev Rheumatol.* (2014) 10:728–39. doi: 10.1038/nrrheum.2014.149
13. Sisson TH, Mendez M, Choi K, Subbotina N, Courey A, Cunningham A, et al. Targeted injury of type II alveolar epithelial cells induces pulmonary fibrosis. *Am J Respir Crit Care Med.* (2010) 181:254–63. doi: 10.1164/rccm.200810-1615OC
14. Plataki M, Koutsopoulos AV, Darivianaki K, Delides G, Siafakas NM, Bouras D. Expression of apoptotic and antiapoptotic markers in epithelial cells in idiopathic pulmonary fibrosis. *Chest.* (2005) 127:266–74. doi: 10.1378/chest.127.1.266
15. Byrne AJ, Maher TM, Lloyd CM. Pulmonary macrophages: a new therapeutic pathway in fibrosing lung disease? *Trends Mol Med.* (2016) 22:303–16. doi: 10.1016/j.molmed.2016.02.004
16. Aran D, Looney AP, Liu L, Wu E, Fong V, Hsu A, et al. Reference-based analysis of lung single-cell sequencing reveals a transitional profibrotic macrophage. *Nature Immunol.* (2019) 20:163–72. doi: 10.1038/s41590-018-0276-y
17. Christmann RB, Sampaio-Barros P, Stifano G, Borges CL, de Carvalho CR, Kairalla R, et al. Association of interferon- and transforming growth factor beta-regulated genes and macrophage activation with systemic sclerosis-related progressive lung fibrosis. *Arthritis Rheumatol.* (2014) 66:714–25. doi: 10.1002/art.38288
18. Schupp JC, Binder H, Jager B, Cillis G, Zissel G, Muller-Quernheim J, et al. Macrophage activation in acute exacerbation of idiopathic pulmonary fibrosis. *PLoS ONE.* (2015) 10:e0116775. doi: 10.1371/journal.pone.0116775
19. Hsu E, Shi H, Jordan RM, Lyons-Weiler J, Pilewski JM, Feghali-Bostwick CA. Lung tissues in systemic sclerosis have gene expression patterns unique to pulmonary fibrosis and pulmonary hypertension. *Arthritis Rheum.* (2011) 63:783–94. doi: 10.1002/art.30159
20. Cai M, Bonella F, He X, Sixt SU, Sarria R, Guzman J, et al. CCL18 in serum, BAL fluid and alveolar macrophage culture supernatant in interstitial lung diseases. *Respir Med.* (2013) 107:1444–52. doi: 10.1016/j.rmed.2013.06.004
21. Mahoney JM, Taroni J, Martyanov V, Wood TA, Greene CS, Pioli PA, et al. Systems level analysis of systemic sclerosis shows a network of immune and profibrotic pathways connected with genetic polymorphisms. *PLoS Comput Biol.* (2015) 11:e1004005. doi: 10.1371/journal.pcbi.1004005
22. Taroni JN, Greene CS, Martyanov V, Wood TA, Christmann RB, Farber HW, et al. A novel multi-network approach reveals tissue-specific cellular modulators of fibrosis in systemic sclerosis. *Genome Med.* (2017) 9:27. doi: 10.1186/s13073-017-0417-1
23. Thomeer MJ, Vansteenkiste J, Verbeke EK, Demedts M. Interstitial lung diseases: characteristics at diagnosis and mortality risk assessment. *Respir Med.* (2004) 98:567–73. doi: 10.1016/j.rmed.2003.10.015
24. Basu S, Zhuang H, Torigian DA, Rosenbaum J, Chen W, Alavi A. Functional imaging of inflammatory diseases using nuclear medicine techniques. *Semin Nucl Med.* (2009) 39:124–45. doi: 10.1053/j.semnuclmed.2008.10.006
25. Hansell DM, Goldin JG, King TE Jr, Lynch DA, Richeldi L, Wells AU. CT staging and monitoring of fibrotic interstitial lung diseases in clinical practice and treatment trials: a position paper from the Fleischner Society. *Lancet Respir Med.* (2015) 3:483–96. doi: 10.1016/S2213-2600(15)00096-X
26. Goldin J, Elashoff R, Kim HJ, Yan X, Lynch D, Strollo D, et al. Treatment of scleroderma-interstitial lung disease with cyclophosphamide is associated with less progressive fibrosis on serial thoracic high-resolution CT scan than placebo: findings from the scleroderma lung study. *Chest.* (2009) 136:1333–40. doi: 10.1378/chest.09-0108
27. Win T, Lambrou T, Hutton BF, Kayani I, Screaton NJ, Porter JC, et al. ¹⁸F-Fluorodeoxyglucose positron emission tomography pulmonary imaging in idiopathic pulmonary fibrosis is reproducible: implications for future clinical trials. *Eur J Nucl Med Mol Imaging.* (2012) 39:521–8. doi: 10.1007/s00259-011-1986-7
28. Nobashi T, Kubo T, Nakamoto Y, Handa T, Koyasu S, Ishimori T, et al. ¹⁸F-FDG uptake in less affected lung field provides prognostic stratification in patients with interstitial lung disease. *J Nucl Med.* (2016) 57:1899–904. doi: 10.2967/jnumed.116.174946
29. Bellando-Randone S, Tartarelli L, Cavigli E, Tofani L, Bruni C, Lepri G, et al. ¹⁸F-fluorodeoxyglucose positron-emission tomography/CT and lung involvement in systemic sclerosis. *Ann Rheum Dis.* (2018) 78:577–8. doi: 10.1136/annrheumdis-2018-eular.3748
30. Bondue B, Castiaux A, Van Sinaeys G, Mathey C, Sherer F, Egrise D, et al. Absence of early metabolic response assessed by ¹⁸F-FDG PET/CT after initiation of antifibrotic drugs in IPF patients. *Respir Res.* (2019) 20:10. doi: 10.1186/s12931-019-0974-5
31. Desogere P, Tapias LF, Hariri LP, Rotile NJ, Rietz TA, Probst CK, et al. Type I collagen-targeted PET probe for pulmonary fibrosis detection and staging in preclinical models. *Sci Transl Med.* (2017) 9:eaa4696. doi: 10.1126/scitranslmed.aaf4696
32. Golestani R, Razavian M, Ye Y, Zhang J, Jung JJ, Toczek J, et al. Matrix metalloproteinase-targeted imaging of lung inflammation and remodeling. *J Nucl Med.* (2017) 58:138–43. doi: 10.2967/jnumed.116.176198
33. Schniering J, Benesova M, Brunner M, Haller S, Cohrs S, Frauenfelder T, et al. Visualisation of interstitial lung disease by molecular imaging of integrin $\alpha_v\beta_3$ and somatostatin receptor 2. *Ann Rheum Dis.* (2019) 78:218–27. doi: 10.1136/annrheumdis-2018-214322
34. Schniering J, Borgna F, Siwowska K, Benesova M, Cohrs S, Hasler R, et al. *In vivo* labeling of plasma proteins for imaging of enhanced vascular permeability in the lungs. *Mol Pharm.* (2018) 15:4995–5004. doi: 10.1021/acs.molpharmaceut.8b00606
35. Schniering J, Guo L, Brunner M, Schibli R, Ye S, Distler O, et al. Evaluation of ^{99m}Tc-rhAnnexin V-128 SPECT/CT as a diagnostic tool for early stages of interstitial lung disease associated with systemic sclerosis. *Arthritis Res Ther.* (2018) 20:183. doi: 10.1186/s13075-018-1681-1
36. Withana NP, Ma X, McGuire HM, Verdoes M, van der Linden WA, Ofori LO, et al. Non-invasive imaging of idiopathic pulmonary fibrosis using cathepsin protease probes. *Sci Rep.* (2016) 6:19755. doi: 10.1038/srep19755
37. Han W, Zaynagetdinov R, Yull FE, Polosukhin VV, Gleaves LA, Tanjore H, et al. Molecular imaging of folate receptor beta-positive macrophages during acute lung inflammation. *Am J Respir Cell Mol Biol.* (2015) 53:50–9. doi: 10.1165/rccb.2014-0289OC
38. Paulos CM, Turk MJ, Breur GJ, Low PS. Folate receptor-mediated targeting of therapeutic and imaging agents to activated macrophages in rheumatoid arthritis. *Adv Drug Deliv Rev.* (2004) 56:1205–17. doi: 10.1016/j.addr.2004.01.012
39. Low PS, Kularatne SA. Folate-targeted therapeutic and imaging agents for cancer. *Curr Opin Chem Biol.* (2009) 13:256–62. doi: 10.1016/j.cbpa.2009.03.022
40. Nagai T, Tanaka M, Hasui K, Shirahama H, Kitajima S, Yonezawa S, et al. Effect of an immunotoxin to folate receptor beta on bleomycin-induced experimental pulmonary fibrosis. *Clin Exp Immunol.* (2010) 161:348–56. doi: 10.1111/j.1365-2249.2010.04182.x
41. Silvola JMU, Li XG, Virta J, Marjamaki P, Liljenback H, Hytonen JP, et al. Aluminum fluoride-18 labeled folate enables *in vivo* detection of atherosclerotic plaque inflammation by positron emission tomography. *Sci Rep.* (2018) 8:9720. doi: 10.1038/s41598-018-27618-4
42. Piscaer TM, Müller C, Mindt TL, Lubberts E, Verhaar JA, Krenning EP, et al. Imaging of activated macrophages in experimental osteoarthritis using folate-targeted animal single-photon-emission computed tomography/computed tomography. *Arthritis Rheum.* (2011) 63:1898–907. doi: 10.1002/art.30363
43. Jager NA, Westra J, Golestani R, van Dam GM, Low PS, Tio RA, et al. Folate receptor-beta imaging using ^{99m}Tc-folate to explore distribution of polarized macrophage populations in human atherosclerotic plaque. *J Nucl Med.* (2014) 55:1945–51. doi: 10.2967/jnumed.114.143180
44. Chandrupatla D, Jansen G, Mantel E, Low PS, Matsuyama T, Musters RP, et al. Imaging and methotrexate response monitoring of systemic inflammation in arthritic rats employing the macrophage PET Tracer [¹⁸F]Fluoro-PEG-Folate. *Contrast Media Mol Imaging.* (2018) 2018:8092781. doi: 10.1155/2018/8092781
45. Ayala-Lopez W, Xia W, Varghese B, Low PS. Imaging of atherosclerosis in apolipoprotein e knockout mice: targeting of a folate-conjugated

- radiopharmaceutical to activated macrophages. *J Nucl Med.* (2010) 51:768–74. doi: 10.2967/jnumed.109.071324
46. Winkel LC, Groen HC, van Thiel BS, Müller C, van der Steen AF, Wentzel JJ, et al. Folate receptor-targeted single-photon emission computed tomography/computed tomography to detect activated macrophages in atherosclerosis: can it distinguish vulnerable from stable atherosclerotic plaques? *Mol Imaging.* (2014) 13. doi: 10.2310/7290.2013.00061
 47. Kelderhouse LE, Robins MT, Rosenbalm KE, Hoylman EK, Mahalingam S, Low PS. Prediction of response to therapy for autoimmune/inflammatory diseases using an activated macrophage-targeted radioimaging agent. *Mol Pharm.* (2015) 12:3547–55. doi: 10.1021/acs.molpharmaceut.5b00134
 48. Kraus VB, McDaniel G, Huebner JL, Stabler TV, Pieper CF, Shipes SW, et al. Direct in vivo evidence of activated macrophages in human osteoarthritis. *Osteoarthr Cartilage.* (2016) 24:1613–21. doi: 10.1016/j.joca.2016.04.010
 49. Papadopoulos V, Baraldi M, Guilarte TR, Knudsen TB, Lacapere JJ, Lindemann P, et al. Translocator protein (18kDa): new nomenclature for the peripheral-type benzodiazepine receptor based on its structure and molecular function. *Trends Pharmacol Sci.* (2006) 27:402–9. doi: 10.1016/j.tips.2006.06.005
 50. Largeau B, Dupont AC, Guilloteau D, Santiago-Ribeiro MJ, Arlicot N. TSPO PET imaging: from microglial activation to peripheral sterile inflammatory diseases? *Contrast Media Mol Imaging.* (2017) 2017:6592139. doi: 10.1155/2017/6592139
 51. Canat X, Guillaumont A, Bouaboula M, Poinot-Chazel C, Derocq JM, Carayon P, et al. Peripheral benzodiazepine receptor modulation with phagocyte differentiation. *Biochem Pharmacol.* (1993) 46:551–4. doi: 10.1016/0006-2952(93)90535-5
 52. Owen DR, Yeo AJ, Gunn RN, Song K, Wadsworth G, Lewis A, et al. An 18-kDa translocator protein (TSPO) polymorphism explains differences in binding affinity of the PET radioligand PBR28. *J Cereb Blood Flow Metab.* (2012) 32:1–5. doi: 10.1038/jcbfm.2011.147
 53. Owen DR, Gunn RN, Rabiner EA, Bennacef I, Fujita M, Kreisl WC, et al. Mixed-affinity binding in humans with 18-kDa translocator protein ligands. *J Nucl Med.* (2011) 52:24–32. doi: 10.2967/jnumed.110.079459
 54. Owen DR, Howell OW, Tang SP, Wells LA, Bennacef I, Bergstrom M, et al. Two binding sites for [³H]PBR28 in human brain: implications for TSPO PET imaging of neuroinflammation. *J Cereb Blood Flow Metab.* (2010) 30:1608–18. doi: 10.1038/jcbfm.2010.63
 55. Schiller HB, Fernandez IE, Burgstaller G, Schaab C, Scheltema RA, Schwarzmayr T, et al. Time- and compartment-resolved proteome profiling of the extracellular niche in lung injury and repair. *Mol Syst Biol.* (2015) 11:819. doi: 10.15252/msb.20156123
 56. Misharin AV, Morales-Nebreda L, Mutlu GM, Budinger GR, Perlman H. Flow cytometric analysis of macrophages and dendritic cell subsets in the mouse lung. *Am J Respir Cell Mol Biol.* (2013) 49:503–10. doi: 10.1165/rcmb.2013-0086MA
 57. Ayaub EA, Dubey A, Imani J, Botelhof F, Kolb MRJ, Richards CD, et al. Overexpression of OSM and IL-6 impacts the polarization of pro-fibrotic macrophages and the development of bleomycin-induced lung fibrosis. *Sci Rep.* (2017) 7:13281. doi: 10.1038/s41598-017-13511-z
 58. Ashcroft T, Simpson JM, Timbrell V. Simple method of estimating severity of pulmonary fibrosis on a numerical scale. *J Clin Pathol.* (1988) 41:467–70. doi: 10.1136/jcp.41.4.467
 59. Seger S, Stritt M, Vezzali E, Nayler O, Hess P, Groenen PMA, et al. A fully automated image analysis method to quantify lung fibrosis in the bleomycin-induced rat model. *PLoS ONE.* (2018) 13:e0193057. doi: 10.1371/journal.pone.0193057
 60. Woessner JF Jr, Boucek RJ. Connective tissue development in subcutaneously implanted polyvinyl sponge. I. Biochemical changes during development. *Arch Biochem Biophys.* (1961) 93:85–94. doi: 10.1016/0003-9861(61)90319-8
 61. Betzel T, Müller C, Groehn V, Müller A, Reber J, Fischer CR, et al. Radiosynthesis and preclinical evaluation of 3'-Aza-2'-[¹⁸F]fluorofolic acid: a novel PET radiotracer for folate receptor targeting. *Bioconjug Chem.* (2013) 24:205–14. doi: 10.1021/bc300483a
 62. Boss SD, Müller C, Siwowska K, Schmid RM, Groehn V, Schibli R, et al. Diastereomerically pure 6R- and 6S-3'-Aza-2'-¹⁸F-Fluoro-5-Methyltetrahydrofolates show unprecedentedly high uptake in folate receptor-positive KB tumors. *J Nucl Med.* (2019) 60:135–41. doi: 10.2967/jnumed.118.213314
 63. Xia W, Hilgenbrink AR, Matteson EL, Lockwood MB, Cheng JX, Low PS. A functional folate receptor is induced during macrophage activation and can be used to target drugs to activated macrophages. *Blood.* (2009) 113:438–46. doi: 10.1182/blood-2008-04-150789
 64. van den Brule S, Huaux F, Uwambayinema F, Ibouaaden S, Yakoub Y, Palmari-Pallag M, et al. Lung inflammation and thymic atrophy after bleomycin are controlled by the prostaglandin D2 receptor DP1. *Am J Respir Cell Mol Biol.* (2014) 50:212–22. doi: 10.1165/rcmb.2012-0520OC
 65. Bellomo A, Gentek R, Bajenoff M, Baratin M. Lymph node macrophages: scavengers, immune sentinels and trophic effectors. *Cell Immunol.* (2018) 330:168–74. doi: 10.1016/j.cellimm.2018.01.010
 66. Junt T, Moseman EA, Iannacone M, Massberg S, Lang PA, Boes M, et al. Subcapsular sinus macrophages in lymph nodes clear lymph-borne viruses and present them to antiviral B cells. *Nature.* (2007) 450:110–4. doi: 10.1038/nature06287
 67. Groves AM, Win T, Screaton NJ, Berovic M, Endozo R, Booth H, et al. Idiopathic pulmonary fibrosis and diffuse parenchymal lung disease: implications from initial experience with ¹⁸F-FDG PET/CT. *J Nucl Med.* (2009) 50:538–45. doi: 10.2967/jnumed.108.057901
 68. Win T, Screaton NJ, Porter JC, Ganeshan B, Maher TM, Fraioli F, et al. Pulmonary ¹⁸F-FDG uptake helps refine current risk stratification in idiopathic pulmonary fibrosis (IPF). *Eur J Nucl Med Mol Imaging.* (2018) 45:806–15. doi: 10.1007/s00259-017-3917-8
 69. Win T, Thomas BA, Lambrou T, Hutton BF, Screaton NJ, Porter JC, et al. Areas of normal pulmonary parenchyma on HRCT exhibit increased FDG PET signal in IPF patients. *Eur J Nucl Med Mol Imaging.* (2014) 41:337–42. doi: 10.1007/s00259-013-2514-8
 70. Justet A, Laurent-Bellue A, Thabut G, Dieudonne A, Debray MP, Borie R, et al. [¹⁸F]FDG PET/CT predicts progression-free survival in patients with idiopathic pulmonary fibrosis. *Respir Res.* (2017) 18:74. doi: 10.1186/s12931-017-0556-3
 71. Motegi SI, Fujiwara C, Sekiguchi A, Hara K, Yamaguchi K, Maeno T, et al. Clinical value of ¹⁸F-fluorodeoxyglucose positron emission tomography/computed tomography for interstitial lung disease and myositis in patients with dermatomyositis. *J Dermatol.* (2019) 46:213–8. doi: 10.1111/1346-8138.14758
 72. Bondue B, Sherer F, Van Simaëys G, Doumont G, Egrise D, Yakoub Y, et al. PET/CT with ¹⁸F-FDG- and ¹⁸F-FBEM-labeled leukocytes for metabolic activity and leukocyte recruitment monitoring in a mouse model of pulmonary fibrosis. *J Nucl Med.* (2015) 56:127–32. doi: 10.2967/jnumed.114.147421
 73. Khanna D, Tashkin DP, Denton CP, Lubell MW, Vazquez-Mateo C, Wax S. Ongoing clinical trials and treatment options for patients with systemic sclerosis-associated interstitial lung disease. *Rheumatology.* (2018) 58:567–79. doi: 10.1093/rheumatology/key151
 74. Kolb M, Bonella F, Wollin L. Therapeutic targets in idiopathic pulmonary fibrosis. *Respir Med.* (2017) 131:49–57. doi: 10.1016/j.rmed.2017.07.062
 75. Distler O, Highland KB, Gahlemann M, Azuma A, Fischer A, Mayes MD, et al. Nintedanib for systemic sclerosis-associated interstitial lung disease. *N Engl J Med.* (2019) 380:2518–28. doi: 10.1056/NEJMoa1903076
 76. Huang J, Maier C, Zhang Y, Soare A, Dees C, Beyer C, et al. Nintedanib inhibits macrophage activation and ameliorates vascular and fibrotic manifestations in the Fra2 mouse model of systemic sclerosis. *Ann Rheum Dis.* (2017) 76:1941–8. doi: 10.1136/annrheumdis-2016-210823
 77. Toda M, Mizuguchi S, Minamiyama Y, Yamamoto-Oka H, Aota T, Kubo S, et al. Pirfenidone suppresses polarization to M2 phenotype macrophages and the fibrogenic activity of rat lung fibroblasts. *J Clin Biochem Nutr.* (2018) 63:58–65. doi: 10.3164/jcbs.17-111
 78. Khanna D, Denton CP, Lin CJF, van Laar JM, Frech TM, Anderson ME, et al. Safety and efficacy of subcutaneous tocilizumab in systemic sclerosis: results from the open-label period of a phase II randomised controlled trial (faSScinate). *Ann Rheum Dis.* (2018) 77:212–20. doi: 10.1136/annrheumdis-2017-211682
 79. Byrne AJ, Mathie SA, Gregory LG, Lloyd CM. Pulmonary macrophages: key players in the innate defence of the airways. *Thorax.* (2015) 70:1189–96. doi: 10.1136/thoraxjnl-2015-207020

80. Li H, Nagai T, Hasui K, Matsuyama T. Depletion of folate receptor beta-expressing macrophages alleviates bleomycin-induced experimental skin fibrosis. *Mod Rheumatol*. (2014) 24:816–22. doi: 10.3109/14397595.2013.879415
81. Feng Y, Shen J, Streaker ED, Lockwood M, Zhu Z, Low PS, et al. A folate receptor beta-specific human monoclonal antibody recognizes activated macrophage of rheumatoid patients and mediates antibody-dependent cell-mediated cytotoxicity. *Arthritis Res Ther*. (2011) 13:R59. doi: 10.1186/ar3312
82. Lynn RC, Feng Y, Schutsky K, Poussin M, Kalota A, Dimitrov DS, et al. High-affinity FRbeta-specific CAR T cells eradicate AML and normal myeloid lineage without HSC toxicity. *Leukemia*. (2016) 30:1355–64. doi: 10.1038/leu.2016.35
83. Cao Z, Lis R, Ginsberg M, Chavez D, Shido K, Rabbany SY, et al. Targeting of the pulmonary capillary vascular niche promotes lung alveolar repair and ameliorates fibrosis. *Nat Med*. (2016) 22:154–62. doi: 10.1038/nm.4035
84. Chen DL, Cheriyan J, Chilvers ER, Choudhury G, Coello C, Connell M, et al. Quantification of lung PET images: challenges and opportunities. *J Nucl Med*. (2017) 58:201–7. doi: 10.2967/jnumed.116.184796
85. Guerra L, Ponti E, Morzenti S, Spadavecchia C, Crivellaro C. Respiratory motion management in PET/CT: applications and clinical usefulness. *Curr Radiopharm*. (2017) 10:85–92. doi: 10.2174/1874471010666170519165918
86. Reddy JA, Xu LC, Parker N, Vetzal M, Leamon CP. Preclinical evaluation of ^{99m}Tc-EC20 for imaging folate receptor-positive tumors. *J Nucl Med*. (2004) 45:857–66.
87. Vande Velde G, Poelmans J, De Langhe E, Hillen A, Vanoirbeek J, Himmelreich U, et al. Longitudinal micro-CT provides biomarkers of lung disease that can be used to assess the effect of therapy in preclinical mouse models, and reveal compensatory changes in lung volume. *Dis Models Mech*. (2016) 9:91–8. doi: 10.1242/dmm.020321
88. Aichler M, Kunzke T, Buck A, Sun N, Ackermann M, Jonigk D, et al. Molecular similarities and differences from human pulmonary fibrosis and corresponding mouse model: MALDI imaging mass spectrometry in comparative medicine. *Lab Invest*. (2018) 98:141–9. doi: 10.1038/labinvest.2017.110

Conflict of Interest: ¹⁸F-AzaFol is patent pending (WO 2013/167653 A1) and the patent is owned by Merck & Cie, Switzerland, an affiliate of Merck KGaA, Darmstadt, Germany. RS and CM are co-inventor on this patent. RS received funding for the development of ¹⁸F-AzaFol from Innosuisse (grant no.: CTI-Project 13877.1 PFLS-LS). CM received funding from Merck & Cie for the performance of preclinical studies with ¹⁸F-AzaFol. OD had consultancy relationships with Actelion, AnaMar, Bayer, Boehringer Ingelheim, Catenion, CSL Behring, ChemomAb, Roche, GSK, Inventiva, Italfarmaco, Lilly, medac, Medscape, Mitsubishi Tanabe Pharma, MSD, Novartis, Pfizer, Sanofi, and UCB in the area of potential treatments of scleroderma and its complications. Additionally, OD has research funding from Actelion, Bayer, Boehringer Ingelheim, Mitsubishi Tanabe Pharma, and Roche. In addition, OD has a patent mir-29 for the treatment of systemic sclerosis registered. BM had grant/research support from AbbVie, Protagen, Novartis, congress support from Pfizer, Roche, and Actelion. In addition, BM has a patent mir-29 for the treatment of systemic sclerosis registered. The real or perceived potential conflicts listed above are accurately stated.

The remaining authors declare that the research was conducted in the absence of any commercial or financial relationships that could be construed as a potential conflict of interest.

Copyright © 2019 Schniering, Benešová, Brunner, Haller, Cohrs, Frauenfelder, Vrugt, Feghali-Bostwick, Schibli, Distler, Müller and Maurer. This is an open-access article distributed under the terms of the Creative Commons Attribution License (CC BY). The use, distribution or reproduction in other forums is permitted, provided the original author(s) and the copyright owner(s) are credited and that the original publication in this journal is cited, in accordance with accepted academic practice. No use, distribution or reproduction is permitted which does not comply with these terms.